Coastal Engineering, 20 (1993) 317–342
Elsevier Science Publishers B.V., Amsterdam

Wave boundary layers in a convergent tunnel

B.M. Sumer, T.S. Laursen and J. Fredsøe
Technical University of Denmark, Institute of Hydrodynamics and Hydraulic Engineering, 2800 Lyngby, Denmark

(Received 26 January 1993; accepted after revision 3 June 1993)

ABSTRACT

This work deals with turbulent oscillatory boundary layers in a convergent–divergent channel with smooth walls. Two kinds of measurements were conducted: velocity measurements and wall shear-stress measurements. Most of the measurements were conducted for three different values of the half-angle of divergence β, namely 0°, 0.5° and 1°. Two other parameters which govern the flow are the Reynolds number, Re, and the parameter a/D where a is the amplitude of water particles at the center of the channel and D is the half-width of the channel. In the tests Re was maintained constant, approximately at $Re=6\times10^6$, while a/D was varied over a range from about 20 to 39 in most of the experiments.

The results indicate that there exists a constant streaming near the wall in the direction towards the convergent end of the channel. The magnitude of this streaming increases with β and also with the distance from the divergent end of the channel. The results further indicate that the friction coefficient increases with β for the convergent half period and decreases with it for the divergent half period. Regarding the turbulence, the experiments show that turbulence is largely suppressed in the convergent half period; this is felt even in the early stage of the following divergent half period. It recovers, however, shortly after and an immense growth in turbulence is observed for the rest of the divergent half period of the flow.

LIST OF SYMBOLS

a	Amplitude of the motion at the center-line of the channel (Eqs. 1 and 2).
D	Half-width of the channel.
f	Friction coefficient (Eqs. 9, 10 and 11).
Re	Reynolds number ($=aU_m/\nu$).
t	Time.
T	Period of the oscillatory flow.
u	Streamwise component of the velocity.
$\bar{u}^+$	$\bar{u}$ normalized by U_f.
u'	Fluctuating component of u.
U	Velocity at the centerline of the channel.
U_m	Maximum value of the velocity at the center-line of the channel.
U_f	Wall shear-stress velocity.

U_{fm} Maximum value of the wall shear-stress velocity.
v Vertical component of the velocity.
v' Fluctuating component of v.
x Streamwise distance defined in Fig. 1.
y Vertical distance from the wall.
y^+ y normalized by ν/U_f.
β Half-angle of the divergence of the channel.
ν Kinematic viscosity.
ρ Fluid density.
τ_0 Wall shear stress.
$\bar{\tau}_{0m}$ Maximum value of $\bar{\tau}_0$.
τ_0' Fluctuating value of τ_0.
δ Boundary layer thickness (Fig. 17).
ϕ Phase lead of the wall shear stress over U.
$\underline{\omega}$ Angular frequency of oscillatory flow.
$\overline{\quad}$ Ensemble averaging.
$\langle\ \rangle$ Period averaging (Eqs. 7 and 8).

Subscripts
c Convergent half period.
d Divergent half period.

1. INTRODUCTION

Turbulent boundary layers have been studied theoretically as well as experimentally quite extensively in recent years. This is due to the importance of the turbulent boundary layer in relation to transport of sediment in the coastal environment. In order to calculate the sediment transport, two matters are of special importance, namely the wall shear stress and the vertical structure of turbulence.

These two matters have been studied intensively in the experimental work by Hino et al. (1983), Sleath (1987) and Jensen et al. (1989), all three studies being performed in a closed U-tube in order to obtain sufficiently high Reynolds numbers for the development of the turbulence. The measurements agree to a large degree with turbulence modelling of this flow situation as done for example by Davies et al. (1988), Justesen (1988a,b) and Hagatun and Eidsvik (1986). The disadvantage of using a U-tube is that the flow becomes totally uniform in the flow direction whereby the wave-induced streaming occurring in the real wave case as first recognized by Longuet-Higgins (1953) will not appear.

The purpose of the present experimental investigation is to extend the more early investigations on uniform boundary layers to cover the non-uniformity caused by a small bottom slope. The flow environment which has been used in the investigation is still a U-tube, to obtain high Reynolds numbers. For this reason the flow in a convergent–divergent tunnel is studied (see Figs. 1 and 2).

Clearly this only partly simulates the real picture of waves propagating along an uneven bottom. The previously mentioned wave induced streaming will still not be present in the set-up and further the deformation of the waves when propagating is not correctly reproduced in the U-tube.

On the other hand, the present investigation enlightens some very important aspects of the wave boundary layer when the bottom is not horizontal: first of all, the experiments will show the difference in the wall shear stresses when the flow is in the converging phase and when it is in the diverging phase.

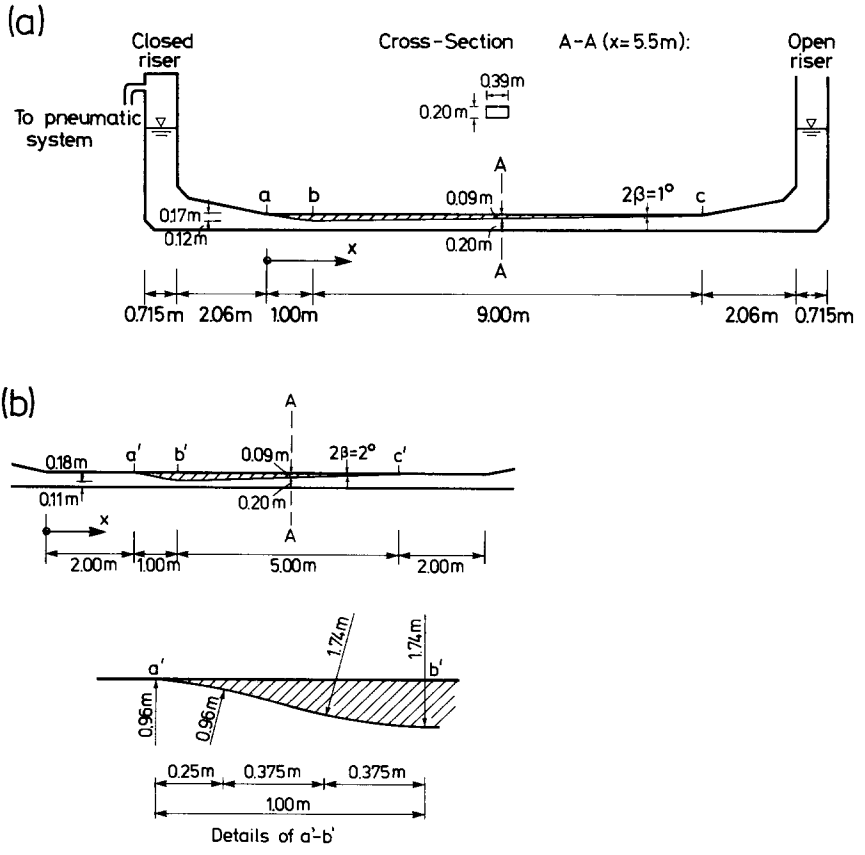

Fig. 1. Schematic description of test set-up. (a) The oscillatory-flow water tunnel with $2\beta=1°$ model. (b) $2\beta=2°$ model and its contraction section.

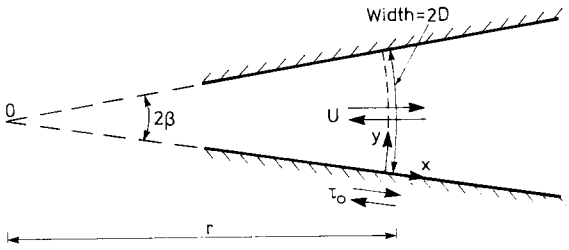

Fig. 2. Definition sketch.

This result is of significance in relation to the resulting cross-shore sediment transport. If suspended sediment is the dominant transport mode the changes in the turbulence structure between the converging and diverging stage also becomes of importance. Finally, the non-uniformity will also involve the presence of a steady streaming, which also can result in a net cross-shore transport.

For the above mentioned reason the present investigation concentrates on the following features of the flow: wall shear stresses, mean flow, streaming and turbulence properties.

Regarding steady, turbulent boundary layer flows in divergent and convergent channels, there are great many works in literature, both theoretical and experimental, reporting on various aspects of the flow (Townsend, 1961; Jonsson, 1968; McDonald, 1969; Engelund, 1973; Kader and Yaglom, 1978; Engelund, 1981).

The similar unsteady flow situation has until now not drawn the same attention, however. On the theoretical side, Justesen (1988a) has modelled the flow situation for the rough wall case by use of a two-equation k–ϵ model, while, to the authors knowledge, no experimental investigations on oscillatory flow in a divergent–convergent tunnel have been carried out.

2. EXPERIMENTAL SET-UP

The experiments were carried out in the U-shaped, oscillatory-flow water tunnel described by Jensen et al. (1989). Two wedge-shaped models were used to establish the convergent–divergent channel in the tunnel, as illustrated in Fig. 1. The half-angle between the walls of the convergent–divergent channel is $\beta = 0.5°$ in one case and $\beta = 1°$ in the other. Both models were made of PVC plastic.

In the present experiment, the bottom of the tunnel was the same as the smooth-bed section of the test set up described by Jensen et al. (1989).

Two kinds of measurements were conducted in the study: the velocity measurements and the wall shear stress measurements. The velocity distribution

over the depth was measured by a two-component Dantec laser Doppler anemometer (LDA). The LDA system was a Dantec two-colour high-performance fibre-optic system with a Dantec 60×11 fibre-optic probe head. A 100 mW argon laser was used in forward scatter mode with two Dantec 55N10 frequency shifters and two Dantec 55N20 frequency trackers. The wall shear stress, on the other hand, was measured with a Dantec 55R46 hot-film probe which was flush-mounted with the bottom of the tunnel at $x=5.5$ m. The details of the measurements are exactly the same as described by Jensen et al. (1989).

Using a wave gauge, the water level in the open riser of the U-tube was recorded simultaneously with the velocity measurements. This served as a reference signal in the data processing.

Mean values of the quantities are calculated through ensemble averaging. The total number of cycles sampled and the sampling intervals are given in Table 1.

3. TEST CONDITIONS

The test conditions are summarized in Table 1 where u and v are the flow velocities in the x- and y-directions respectively (see Fig. 2). τ_0 is the wall shear stress, T is the period of the oscillatory motion. x is measured from the inlet section at the closed-riser side of the tunnel, as indicated in Fig. 1, while y is measured from the bottom over a circular arc, as indicated in Fig. 2. Further in Table 1, D is the half-width of the convergent–divergent tunnel at section A–A (i.e. $x=5.5$ m, see Fig. 1), U_{md} is the maximum value of the flow velocity measured at the centerline of the channel at section A–A in the diverging half period (or, for $\beta=0°$, in the half period where the flow is from the closed riser to the open riser of the tunnel, see Fig. 1), while U_{mc} is that in the converging half period (or, for $\beta=0°$, in the half period where the flow is from the open riser to the closed riser), and U_m is the average of U_{mc} and U_{md}. The quantities a_d and a_c in the table are the amplitudes of the water motion calculated from

$$a_d=\frac{1}{2\pi}U_{md}T \tag{1}$$

and

$$a_c=\frac{1}{2\pi}U_{mc}T \tag{2}$$

assuming that the flow velocity varies sinusoidally for each half period, i.e. for the divergent half period:

$$U=U_{md}\sin(\omega t) \qquad 0°\leqslant\omega t\leqslant 180° \tag{3}$$

TABLE 1

Test conditions

Test No.	Half angle of the channel β (deg.)	Measur. station (Fig. 1) x (m)	Half width of the channel at the station $x=5.5$ m D (m)	Period T (s)	Maximum velocity at $x=5.5$ m at the center line of the convergent–divergent section			Amplitude of the oscillatory motion at $x=5.5$ at the center line of the convergent–divergent section		
					U_{mc} In the conv. half period (m/s)	U_{md} In the div. half period (m/s)	U_m Average (m/s)	a_c In the conv. half period (m)	a_d In the div. half period (m)	a Average (m)
1	0	5.5	0.145	9.5	1.90	1.97	1.935	2.87	2.98	2.93
2	0.5	5.5	0.10	7.6	2.14	2.33	2.23	2.59	2.63	2.7
3	0.5	5.5	0.10	9.1	1.96	2.21	2.08	2.82	3.18	3.00
4	0.5	5.5	0.10	10.9	1.82	2.07	1.94	3.16	3.59	3.37
5	1	5.5	0.10	6.3	2.36	2.71	2.54	2.36	2.70	2.53
6	1	5.5	0.10	7.6	2.04	2.39	2.22	2.47	2.89	2.68
7	1	5.5	0.10	9.1	1.85	2.16	2.01	2.67	3.13	2.91
8	1	5.5	0.10	10.9	1.77	2.08	1.92	3.07	3.59	3.33
9	1	5.5	0.10	12.2	1.64	1.84	1.74	3.19	3.57	3.38
10	1	5.5	0.10	11.0	1.78	2.08	1.93	3.11	3.64	3.37
11	1	5.5	0.10	13.7	1.56	1.76	1.66	3.41	3.82	3.62
12	1	5.5	0.10	10.8	1.88	1.99	1.94	3.23	3.42	3.33
13	0	5.5	0.145	9.75	2.04	1.98	2.01	3.17	3.07	3.12
14	1	7.95	0.10	9.9	1.78	2.14	1.96	2.80	3.37	3.08
15	1	6.75	0.10	9.9	1.78	2.14	1.96	2.80	3.37	3.08
16	1	5.50	0.10	9.9	1.78	2.14	1.96	2.80	3.37	3.08
17	1	4.25	0.10	9.9	1.78	2.14	1.96	2.80	3.37	3.08

and for the convergent half period:

$$U=U_{mc}\sin(\omega t) \qquad 180^\circ \leqslant \omega t \leqslant 360^\circ \tag{4}$$

in which ω is the angular frequency, equal to $2\pi/T$, and t is time. The amplitude a in the table on the other hand is the average of a_c and a_d. As will be shown later, the difference between a_c and a_d (as well as U_{mc} and U_{md}) is due

Normalized amplitude at $x=5.5$ m a/D			Reynolds number $Re=(aU_m)/\nu$	Maximum shear velocity (from direct measurements)		Quantities measured	Apparatus	Number of cycles	Sampling interval (ms)
In the conv. half period	In the div. half period	Average		$U_{fm,c}$ In the conv. half period (cm/s)	$U_{fm,d}$ In the div. half period (cm/s)				
20	20.5	20	5.7×10^6	8.5	8.65	$\bar{\tau}_0$, $(\overline{\tau_0'^2})^{1/2}$	hot film	50	48
26	28	27	6.1×10^6	9.6	9.15	$\bar{\tau}_0$, $(\overline{\tau_0'^2})^{1/2}$	hot film	50	48
29	30.5	30	6.2×10^6	9.3	8.7	$\bar{\tau}_0$, $(\overline{\tau_0'^2})^{1/2}$	hot film	50	48
32	36	34	6.5×10^6	8.4	7.9	$\bar{\tau}_0$, $(\overline{\tau_0'^2})^{1/2}$	hot film	50	48
24	27	26	6.4×10^6	10.3	9.5	$\bar{\tau}_0$, $(\overline{\tau_0'^2})^{1/2}$	hot film	50	48
25	29	27	5.9×10^6	9.4	8.9	$\bar{\tau}_0$, $(\overline{\tau_0'^2})^{1/2}$	hot film	50	48
27	32	29.5	5.9×10^6	8.8	8.2	$\bar{\tau}_0$, $(\overline{\tau_0'^2})^{1/2}$	hot film	50	48
31	36.5	34	6.4×10^6	8.4	7.75	$\bar{\tau}_0$, $(\overline{\tau_0'^2})^{1/2}$	hot film	50	48
32	36	34	5.9×10^6	7.9	7.2	$\bar{\tau}_0$, $(\overline{\tau_0'^2})^{1/2}$	hot film	50	48
32	37	34.5	6.5×10^6	8.2	7.7	$\bar{\tau}_0$, $(\overline{\tau_0'^2})^{1/2}$	hot film	50	48
35	39	37	6.0×10^6	7.6	6.6	$\bar{\tau}_0$, $(\overline{\tau_0'^2})^{1/2}$	hot film	50	48
33	35	34	6.5×10^6	–	–	$\bar{u}$, $(\overline{u'^2})^{1/2}$, $(\overline{v'^2})^{1/2}$, $\overline{u'v'}$, $\langle\bar{u}\rangle$	Two-comp. LDA	80	48
22	21	21.5	6.2×10^6	–	–	$\bar{u}$, $(\overline{u'^2})^{1/2}$, $(\overline{v'^2})^{1/2}$, $\overline{u'v'}$, $\langle\bar{u}\rangle$	Two-comp. LDA	80	48
28	34	31	6.0×10^6	–	–	$\langle\bar{u}\rangle$	Two-comp. LDA	50	48
28	34	31	6.0×10^6	–	–	$\langle\bar{u}\rangle$	Two-comp. LDA	50	48
28	34	31	6.0×10^6	–	–	$\langle\bar{u}\rangle$	Two-comp. LDA	50	48
28	34	31	6.0×10^6	–	–	$\langle\bar{u}\rangle$	Two-comp. LDA	50	48

to a streaming which is caused by the convergent–divergent geometry of the channel.

It should be noted that even for the case of $\beta=0°$, because of very small asymmetric movement in the U-tube, there is a slight difference between the maximum velocities in the two half periods. However, the time-averaged velocity in the $\beta=0°$ case was always measured to be not larger than $0.005U_m$ which is small compared to the streaming induced by non-uniformity, as will be seen later.

Furthermore, $U_{fm,c}$ and $U_{fm,d}$ in the table are the maximum wall shear-stress velocities defined by

$$U_{fm,c} = \sqrt{\frac{\bar{\tau}_{0m,c}}{\rho}} \tag{5}$$

and

$$U_{fm,d} = \sqrt{\frac{\bar{\tau}_{0m,d}}{\rho}} \tag{6}$$

in the convergent- and divergent-half periods, respectively. Here ρ is the fluid density, and $\bar{\tau}_{0m,c}$ and $\bar{\tau}_{0m,d}$ are the maximum values of the mean wall shear stress, in the convergent- and divergent-half periods, respectively.

To achieve fully-developed turbulent-flow conditions, the Reynolds number of the experiments was maintained high, namely at approximately 6×10^6. (Our previous work on turbulent oscillatory boundary layer over a plane boundary ($\beta = 0°$) (Jensen et al., 1989) has shown that, even at this Reynolds number, some portion of the half period at the early stage of the flow ($0 < \omega t \lesssim 15°$) is still not fully turbulent). Furthermore, large orbital motion is needed in order to obtain reliable measurements on the period-averaged wall shear stress and flow pattern which comes into existence as a small difference between two large values. Consequently, the amplitude of the oscillatory motion in the experiments was maintained quite high. The largest amplitude is about 3.6 m, as seen from Table 1. That means that the total travel of a fluid particle in this case is 7.2 m, implying that some fluid in the core region of the tunnel travels outside the convergent–divergent test section and then returns to the test section at the end of one period. Clearly, this effect would be felt more for the $\beta = 1°$ situation than for the $\beta = 0.5°$ case due to the relatively shorter model length of the $\beta = 1°$ case, namely 5 m.

To assess the situation, autocorrelation measurements were made of the streamwise component of the center-line velocity at Section A–A in the case of $\beta = 1°$. The centerline velocity signal was high-pass filtered and then the conventional auto-correlation analysis was implemented for the filtered signal, that is, for the signal which represents turbulence at the measurement point. From the obtained auto-correlation information, the time-scale of turbulence, τ, was predicted. The calculations showed that τ is in the order of magnitude of 0.2 s. This implies that fluid particles travelling in the core region do not remember where their trajectories originated for streamwise distances larger than about 2.5 m/s $\times$ 0.2 s = 0.5 m, considering the velocity with which the fluid particles travel is 2.5 m/s. This means that even in the case of $\beta = 1°$, the turbulence measured at the mid-section of the convergent–divergent channel (namely at Section A–A) will not be affected by the relatively short length of the model. Regarding the mean flow, one may argue that the same is true for the mean flow near the bed on the ground that the total travel

of a fluid particle is much smaller than that in the core region of the tunnel, thus the fluid in the near-bed region travels inside the convergent–divergent test section. Regarding the mean flow in the core region, however, some effect must be expected, particularly near the two ends of the convergent–divergent section. This, in effect, may manifest itself to some degree in the long-time averaged constant circulation pattern in the channel.

One other point which needs to be clarified with regard to the end effects concerns the 1 m long contraction section, Section a–b (or a′– b′ for the $2\beta=2°$ model) in Fig. 1.

This section was given a streamline form, as indicated in Fig. 1, to ensure no vortex formation in the half periods where the flow is towards the closed riser. Careful visual observations in the case of $\beta=1°$, using the so-called tuft method (where soft silk threads were attached to the wall), showed, however, no trace of vortex formation behind the model.

4. RESULTS AND DISCUSSION

4.1. Streaming

Fig. 3 gives sample records for the wall shear stress together with the centerline velocity at Section A–A (see Fig. 1) for two cases, namely for the case where $\beta=0°$ (Fig. 3a) and for that where $\beta=1°$ (Fig. 3b). The figure shows that, while there is practically no difference between the two half periods in the case of $\beta=0°$, the shear stresses experienced in the convergent half periods in the case of $\beta=1°$ are distinctly larger than those in the divergent half periods of the motion.

Fig. 4 presents the phase-averaged wall shear stress variation with respect to time for the three half angles tested, namely $\beta=0°$, 0.5° and 1° for Test 1, Test 3 and Test 7, respectively. This figure, again, shows that relatively smaller wall shear stresses are experienced in the divergent half periods for $\beta=0.5°$ and $\beta=1°$. The preceding observations imply that the period-averaged wall shear stress in an oscillatory flow in a convergent–divergent channel must have a non-zero value, where the resulting shear stress is directed towards the converging direction. The latter in turn implies that there must be a constant streaming of fluid near the wall towards the converging end of the channel, as will be demonstrated a little later in the section.

Fig. 5 depicts the period-averaged wall shear stress as function of β. The period-averaged wall shear stress is defined by the following equation

$$\langle \bar{\tau}_0 \rangle = \frac{1}{T}\int_0^T \bar{\tau}_0 \mathrm{d}t \tag{7}$$

The sign convention in the figure is such that positive shear stress is directed towards the divergent end of the channel (Figs. 1 and 2). The figure clearly shows that the period-averaged shear stress is non-zero and its mag-

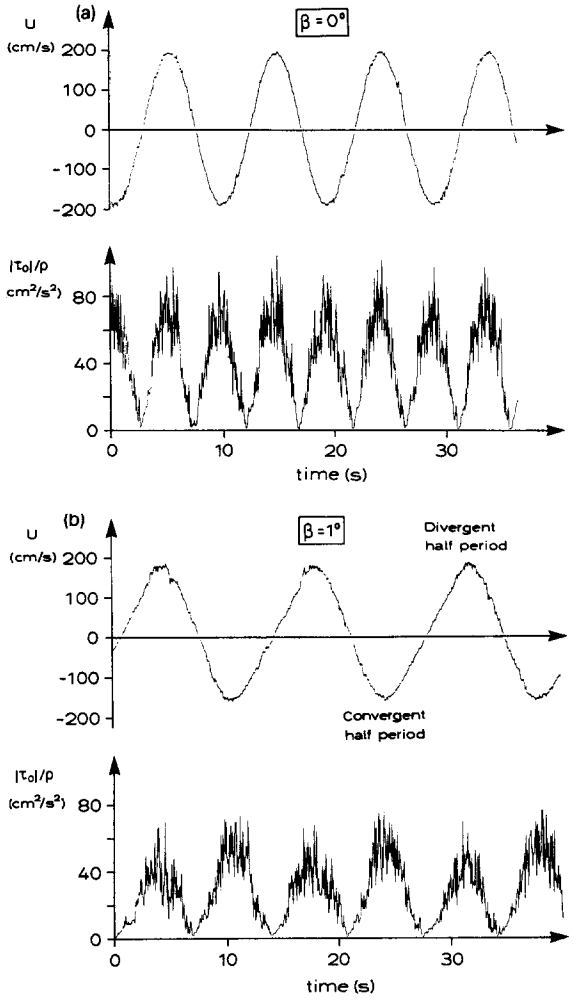

Fig. 3. Sample records of centerline velocity and wall shear stress. Measurements at Section A–A. (a) Test 1; (b) Test 11.

nitude increases with half-angle of the channel, β. Also, the fact that a good correlation is obtained when the data is plotted in the normalized form $\langle \bar{\tau}_0 \rangle / (\rho U_m^2)$ indicates that the period-averaged shear stress scales with the maximum velocity, namely U_m, at the same location. This is in fact expected in analogy with the steady, zero pressure-gradient turbulent boundary-layer flows.

It is well known that in the non-uniform wave boundary layers, the period-averaged velocity $\langle \bar{u} \rangle$ defined by

$$\langle \bar{u} \rangle = \frac{1}{T} \int_0^T \bar{u} dt \tag{8}$$

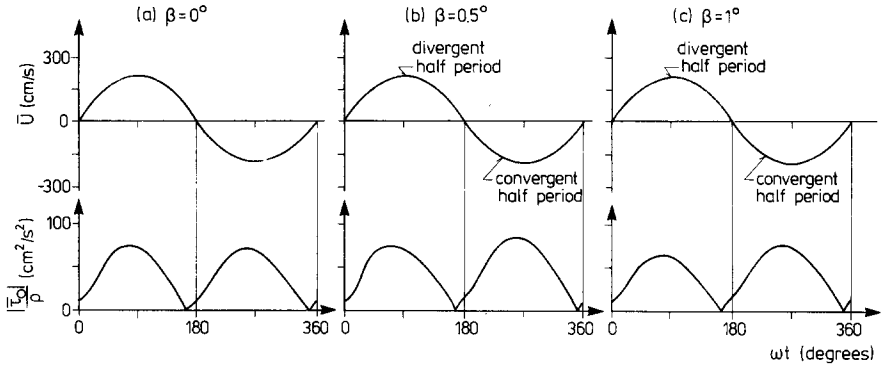

Fig. 4. Mean wall shear stress variation with time. $\bar{u}$ is the mean centerline velocity. (a) Test 1; (b) Test 3; (c) Test 7.

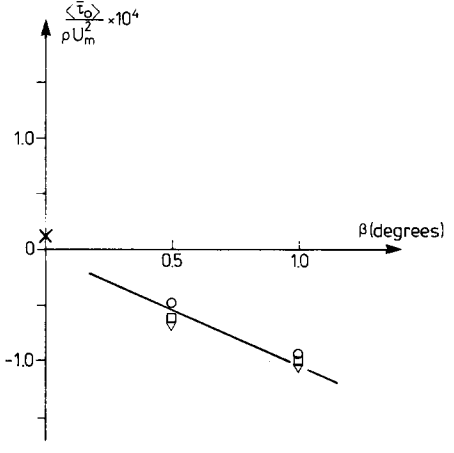

Fig. 5. Period-averaged wall shear stress versus half-angle β. (○) $a/D=27$; (▽) $a/D=30$; (□) $a/D=34$. Re is approximately 6×10^6. Tests 1, 2, 3, 4, 6, 7 and 8. Positive shear stress is directed towards the divergent end of the channel.

becomes different from zero. Here, T is the period of the oscillatory flow. Longuet-Higgins (1957) calculated the streaming under sinusoidal waves due to the non-uniformity of the wave boundary layer caused by the spatial changes of the orbital velocities in real waves (in contrast to the oscillatory flow in uniform pipes etc.). The streaming is introduced also in the present case as implied by Figs. 3, 4 and 5; however the non-uniformity in the present case is caused by the convergent–divergent geometry of the flow environment.

Period-averaged flow in the test section in the case of uniform flow ($\beta=0°$)

In order to assess the significance of the streaming caused by the convergent–divergent geometry of the flow environment, first the period-averaged

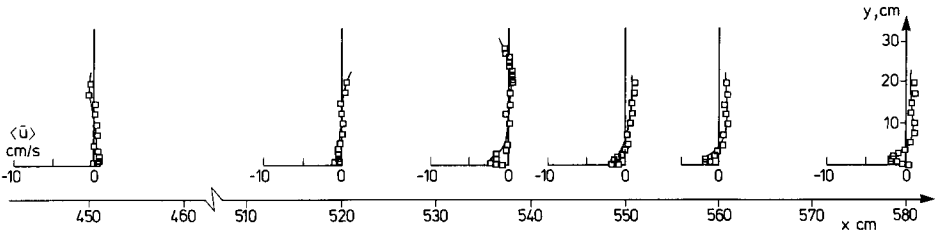

Fig. 6. Period-averaged velocity distributions in the test section in the absence of the convergent–divergent model section, $\beta = 0°$. Test conditions are the same as in Test Series 12.

velocity profiles were measured at several measurement stations in the tunnel in the absence of the test models, i.e. $\beta = 0°$. In these experiments, the flow conditions were maintained the same as in Test 12.

The measured velocity profiles are depicted in Fig. 6. The figure indicates that there is a secondary circulation in the test section. The data in the figure shows that the streaming near the bed associated with this circulation is not larger than 1% of the maximum velocity of the motion (cf. Table 1).

This secondary circulation is caused by the presence of the contraction sections at the two ends of the tunnel. As will be shown in the following section the presence of such convergent–divergent sections in oscillatory boundary-layer flows would cause a streaming near the walls in the direction towards the convergent section.

Fig. 6 further indicates that the reversal of the near-wall flow occurs somewhere between $x = 450$ cm and $x = 520$ cm. This coincides with the mid-section of the tunnel (cf. Fig. 1), and this behaviour must in fact be expected due to symmetry.

Streaming induced by the convergent–divergent geometry of the flow

Fig. 7 presents the period-averaged velocity profiles measured at four different stations as indicated in the figure. The measurements were conducted for only $\beta = 1°$ situation. As is seen clearly, there is a constant streaming near the bed in the direction where the two walls of the channel converge, verifying the argument put forward in the preceding paragraphs in relation to the measured period-averaged wall shear stress. Fig. 7 further indicates that the flow in the converging direction near the wall is balanced by a flow in the opposite direction in the core region of the channel. This implies that there exists a recirculating flow system induced by the convergent–divergent geometry of the channel, as sketched in Fig. 8.

According to the measurements of the period-averaged velocity profiles obtained in the absence of the test models presented in Fig. 6, it has been established that there exists a secondary circulation in the tunnel. The streaming associated with this secondary circulation near the bed is not larger than 1%

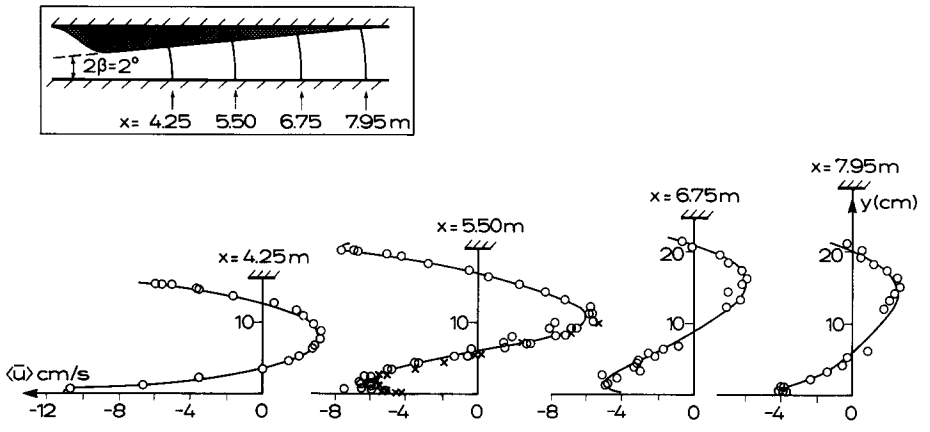

Fig. 7. Period-averaged velocity distributions. *Re* is approximately 6×10^6. (○) Tests 14–17; (×) Test 12.

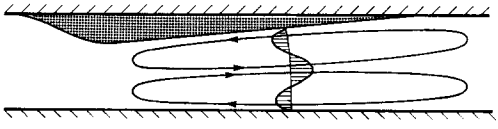

Fig. 8. Sketch of the period-averaged recirculating flow system induced by the convergent–divergent geometry of the channel.

of the maximum velocity of the motion, namely not larger than 2 cm/s, as mentioned previously. A comparison of the streaming velocity near the bed at the inlet section of the convergent–divergent section (at $x=7.95$ m in Fig. 7) with the existing maximum streaming velocity, namely 2 cm/s, indicates that the streaming at this location is in the same order of magnitude as that which is already existing in the tunnel (as implied by the sketch in Fig. 8, the influence of the convergent–divergent geometry of the test section is almost nil in the neighbourhood of the inlet section). However, it is clear from Fig. 7 that the induced streaming due to the convergent–divergent geometry of the channel increases towards the convergent end of the channel. Indeed, at Station $x=4.25$ m, the streaming velocity experienced near the bed becomes a factor 6 larger than the background streaming, as is seen from Fig. 7.

Since the experiments use a channel of finite width, the reversing flow associated with the streaming along the centerline of the channel is strong. In an infinite system, however, the recirculation might be expected to be zero. In such a situation, the maximum values of the outer oscillatory flow velocity, U_{md} and U_{mc}, are identical in each half period, in contrast to the small difference experienced in the present case. This suggests that the near-bed stream-

ing velocities in an infinite system may be expected to be slightly higher than the ones predicted in the present study.

4.2. *Wall friction*

Traditionally, the wall shear stress in oscillatory boundary layers is related to the maximum flow velocity by

$$\bar{\tau}_{0m} = \frac{1}{2} f_w \rho U_m^2 \tag{9}$$

where $\bar{\tau}_{0m}$ is the maximum value of the wall shear stress and f_w is the wave friction coefficient. In the present case, the preceding equation is written for the two half periods separately:

$$\bar{\tau}_{0m,c} = \frac{1}{2} f_c \rho U_{mc}^2 \tag{10}$$

$$\bar{\tau}_{0m,d} = \frac{1}{2} f_d \rho U_{md}^2 \tag{11}$$

where the indices c and d refer to the convergent and divergent half periods, respectively.

From the previous work regarding uniform oscillatory boundary layers (Kamphuis, 1975; Jensen et al., 1989), it is known that the friction coefficient changes with Re

$$Re = \frac{aU_m}{\nu} \tag{12}$$

It can be argued that the Re dependence in the present case may not be extremely different from that indicated by the previous works. Clearly, the major parameter in the present case is the angle β, the half-angle of divergence. Fig. 9 illustrates the effect of β on the friction coefficient. The figure shows that f increases for the convergent half period and decreases for the diverging half period with increasing β, as expected from steady flow.

The distance from the origin r (Fig. 2) should also be involved in the non-dimensional formulation of the friction coefficient.

On dimensional grounds, a/r may then appear to be one other non-dimensional parameter in addition to Re and β. For convenience, however, we may adopt the following combination of the parameters, namely Re, β and a/D, by combining r and β to give $D = r\beta$. Obviously, for a given β, the quantity D plays the same role as r; the larger the distance r, the larger the half-width D.

Fig. 10 presents the friction coefficient data as function of a/D for $\beta = 1°$. Although there is a trend that f increases with increasing a/D for the convergent half period and remains approximately constant within the tested a/D

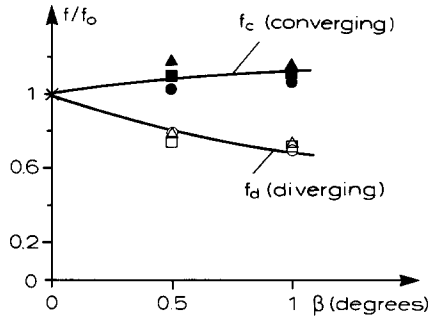

Fig. 9. Friction coefficient versus half-angle β. Circles: $a/D=27$. Triangles: $a/D=30$. Squares: $a/D=34$. Filled symbols: convergent half period. Open symbols: divergent half period. Re is approximately 6×10^6. Tests 1, 2, 3, 4, 6, 7 and 8.

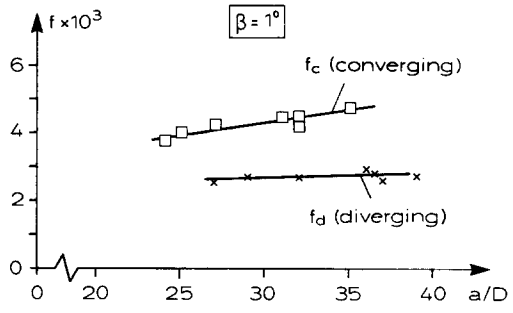

Fig. 10. Friction coefficient versus amplitude-to-half-width ratio. Re is approximately 6×10^6. Tests 5–11.

range for the divergent half period, the tested range of a/D is too small for the results to be conclusive.

The results presented in the preceding paragraphs agree well with Justesen's (1988a) theoretical solutions in a qualitative manner. A direct comparison is not possible, however, due to the fact that Justesen's results are valid only for hydraulically rough walls, as mentioned previously.

Fig. 11 gives the phase lead of the wall shear stress ϕ over the centerline velocity as function of β. From the figure the following points may be noted.

Firstly, the phase lead is larger, in other words the wall shear stress reverses earlier, in the divergent half period than in the convergent half period. This can be attributed to the larger adverse pressure gradient experienced in the divergent half period due to the diverging geometry of the channel.

Secondly, the phase lead for the divergent half period becomes larger and larger, as β increases. Again this can be explained in the same way as in the preceding paragraph. It seems that the phase lead for the convergent half period is not affected much by changing β in the tested range.

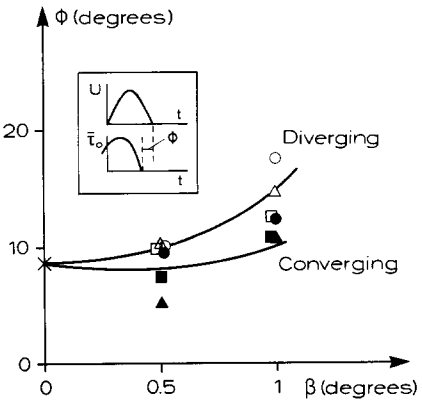

Fig. 11. Phase lead versus half-angle β. Symbols are the same as in Fig. 9.

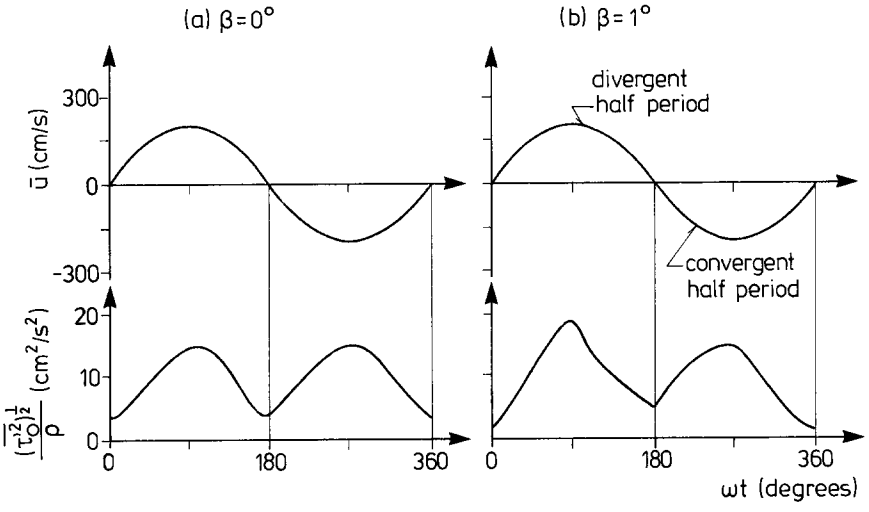

Fig. 12. Time variation of r.m.s. value of wall shear stress fluctuation. (a) Test 1; (b) Test 7.

Finally, Fig. 12 presents the variation of the root-mean-square (r.m.s.) value of the wall shear stress fluctuations, $\sqrt{(\overline{\tau_0'^2})}$, in phase space for two different values of β, namely for $\beta=0°$ and for $\beta=1°$, while Figs. 13 and 14 give the complete data obtained in the present study regarding the r.m.s. value of τ_0'.

From the figures the r.m.s. value of the wall shear stress fluctuations is larger in the divergent half period than in the convergent half period. This indicates that turbulence in the divergent half period is larger than in the convergent half period. The latter issue will be discussed in some detail in the following section in relation to the present turbulence measurements. As will be seen,

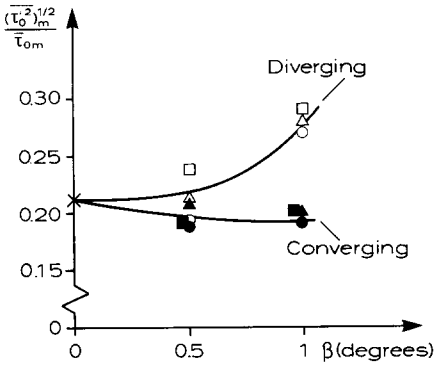

Fig. 13. Maximum of r.m.s. value of wall shear stress fluctuations versus half-angle β. Symbols are the same as in Fig. 9.

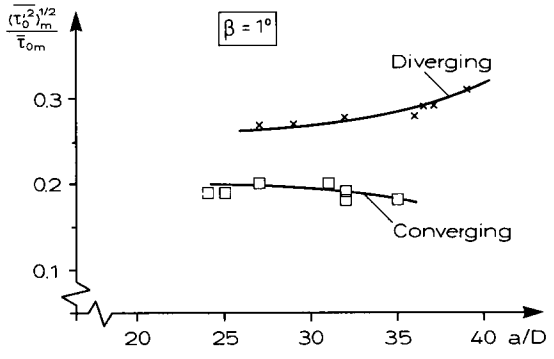

Fig. 14. Maximum of r.m.s. value of wall shear stress versus a/D. Tests 5–11.

the data in Figs. 12–14 will substantiate the turbulence data presented in the following section.

4.3. Mean flow and turbulence

Fig. 15 presents the mean velocity profiles measured at Section A–A ($x=5.5$ m) for various values of ωt during one period of the motion. Fig. 16, on the other hand, presents the profiles for the turbulence quantities $(\overline{u'^2})^{1/2}$, $(\overline{v'^2})^{1/2}$ and $\overline{u'v'}$ measured at the same section. Here u' $(=u-\bar{u})$ and v' $(=v-\bar{v})$ are the fluctuating components of the velocity in x and y directions, respectively. In the figure, the results corresponding to the case of $\beta=0°$ are also plotted for comparison.

From Fig. 16 it is seen that turbulence is greatly suppressed in the convergent half period with respect to that experienced in the case when $\beta=0°$. This is due to the strong, favourable pressure gradient caused by the convergent

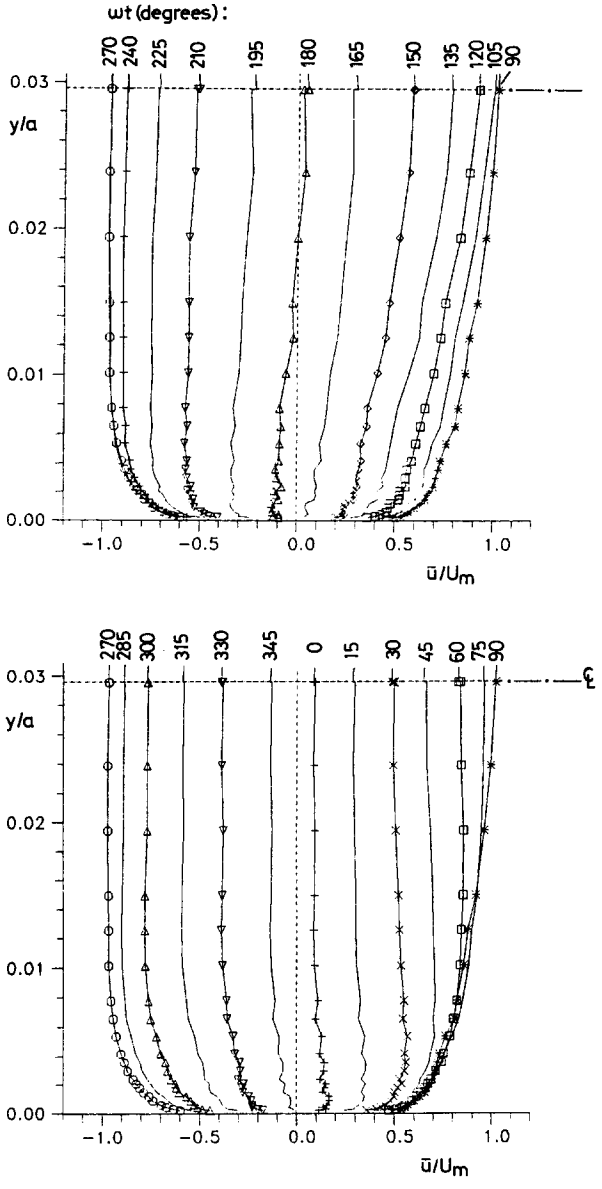

Fig. 15. Mean velocity profiles. $\beta=1°$. *Re* is approximately 6×10^6. Test 12. $\omega t=0°$–$180°$: divergent half period; $\omega t=180°$–$360°$: convergent half period.

geometry of the channel. Fig. 16b indicates that, even in the deceleration stage ($\omega t=270°$–$360°$) where the pressure gradient due to the oscillatory flow changes to an adverse one, the turbulence is still far from recovering at the early stage of the half period. It is only after about $\omega t=60°$ that the turbu-

lence fully recovers (Fig. 16a). Obviously, the recovery of the turbulence is helped by the strong, adverse pressure gradient imposed by the divergent geometry of the channel experienced in this half period.

It is remarkable how the turbulence quantities evolve for $\omega t \lesssim 60°$ in the divergent half period of the flow (Fig. 16a). There is a large increase in the turbulence quantities for this portion of the half period. This is caused by the strong adverse pressure gradient caused by the divergent geometry of the channel and, later in the decelerating stage of the oscillatory motion, by the combined action of the former plus the adverse pressure gradient caused by the deceleration of the flow.

As mentioned previously, the data regarding the wall shear stress fluctuations (Figs. 12–14) substantiate the turbulence data in Fig. 16 in the sense that it, too, clearly shows a large increase in turbulence in the divergent half period.

No measurements of streamwise variation of turbulence quantities have been made in the present study. However, it may be expected that the previously mentioned behaviour, namely the suppression of turbulence in the convergent half period and its immense growth in the divergent half period, would prevail in the channel, with an increasing degree of magnitude towards the convergent end of the channel.

Fig. 17 concerns the time evolution of the boundary layer thickness during the course of the motion. The quantity δ indicated in Fig. 17, may be described as the boundary-layer thickness and, as the figure indicates, δ increases as the half cycle of the motion progresses. However, the figure shows that δ increases violently in the divergent half period after ωt reaches the value of about 60°, which again supports the observation made in the previous figure about the remarkable growth of turbulence for $\omega t \lesssim 60°$ in this half period of the motion.

Fig. 18 presents the mean velocity data normalized by the wall units and plotted in the familiar semi-log form. Here $\bar{u}^+$ and y^+ are defined by

$$\bar{u}^+ = \frac{\bar{u}}{U_f} \qquad \text{and} \qquad y^+ = \frac{yU_f}{\nu} \tag{13}$$

in which U_f is the temporal value of the friction velocity, $U_f = (\bar{\tau}_0/\rho)^{1/2}$. In calculating $\bar{u}^+$ and y^+, the friction velocity U_f is taken as the value measured directly by the wall shear stress probe. Also plotted in Fig. 18 is the steady boundary-layer velocity distribution which is valid close to the wall

$$\bar{u}^+ = 2\int_0^{y^+} \frac{dy^+}{1+\{1+4\kappa^2(y^+)^2[1-\exp(-y^+/A)]^2\}^{1/2}} \tag{14}$$

where κ is the Von Kármán constant ($=0.4$) and A the van Driest damping

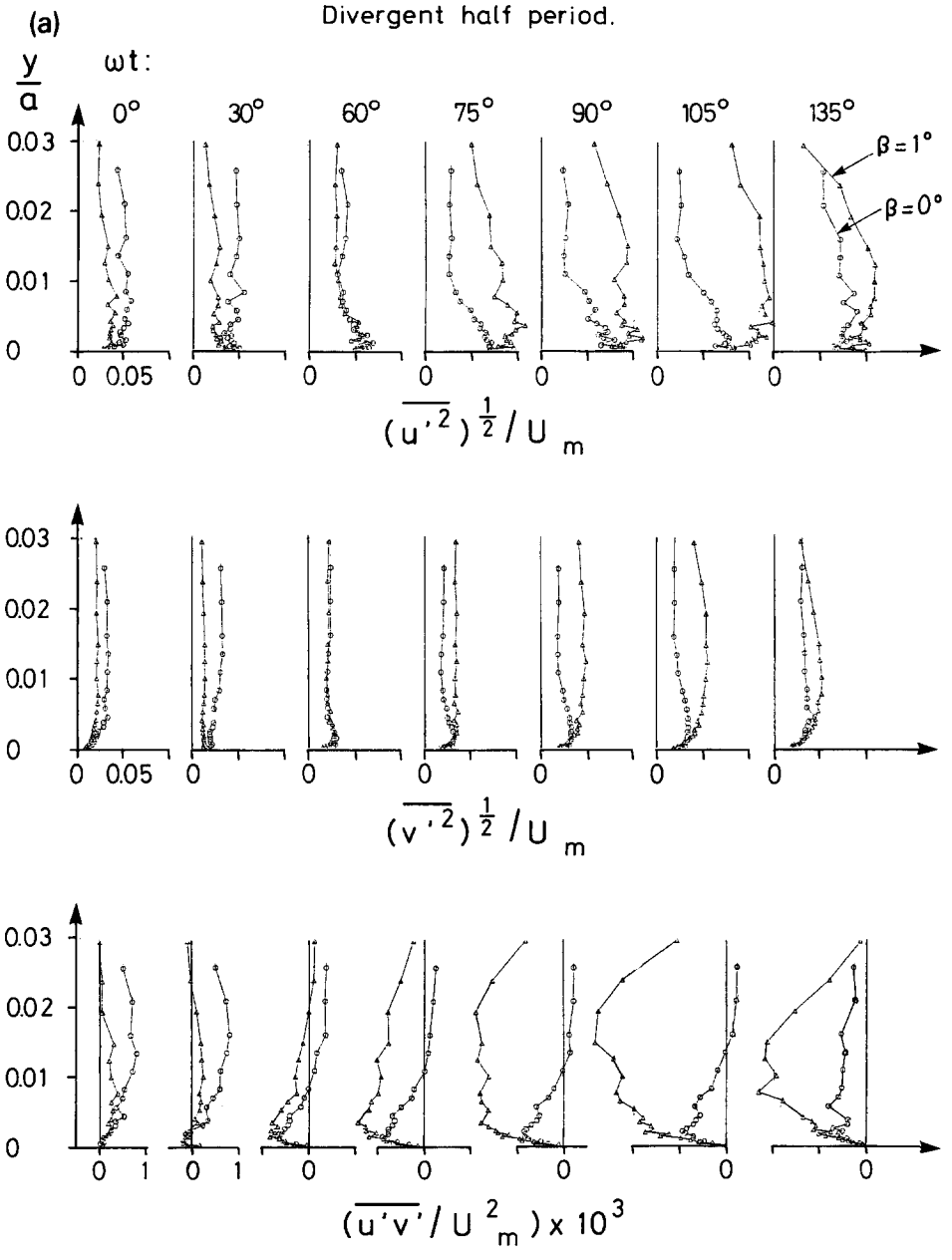

Fig. 16a. Distributions of r.m.s. values of velocity fluctuations u' and v' and also of Reynolds stress $\overline{u'v'}$. (△) $\beta = 1°$. (○) $\beta = 0°$. Re is approximately 6×10^6. Tests 12 and 13. Divergent half period.

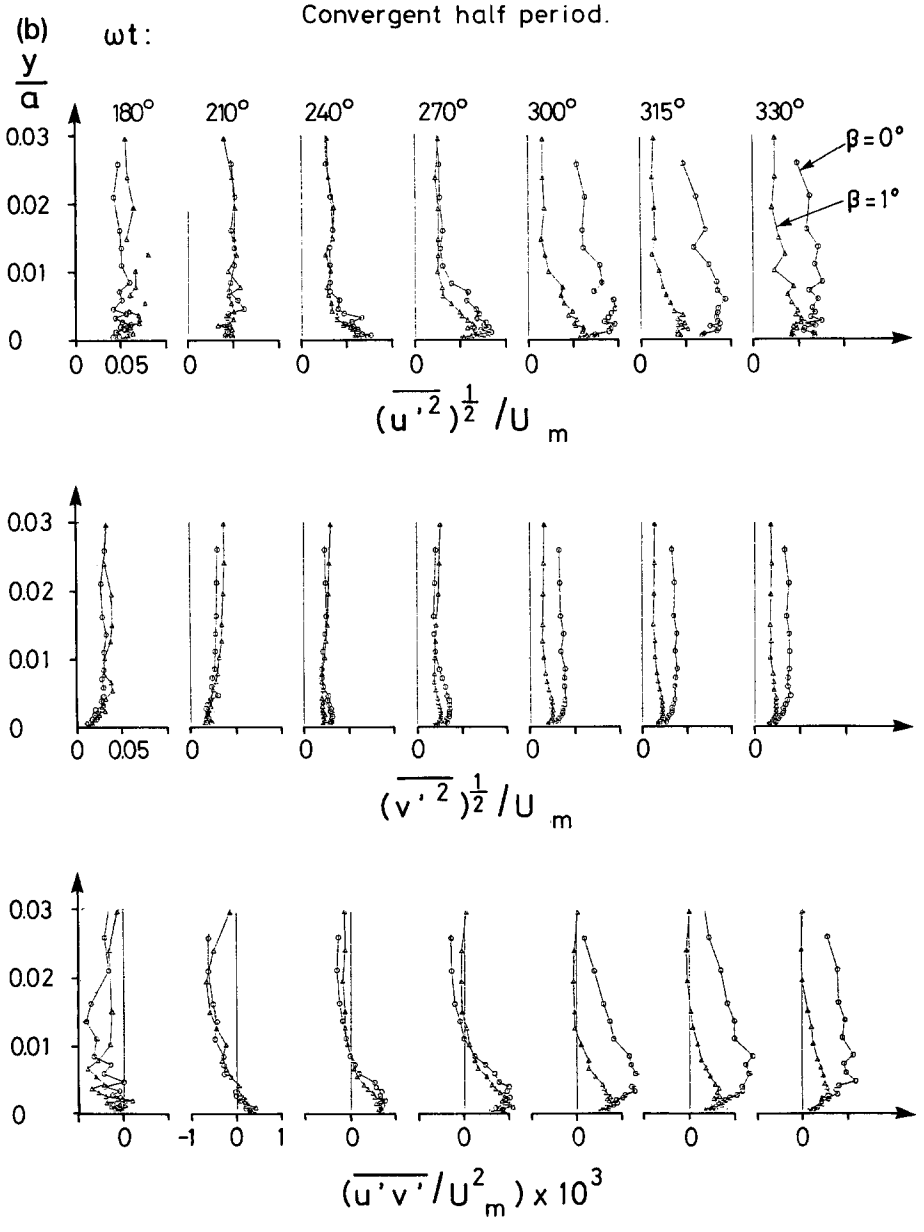

Fig. 16b. Distributions of r.m.s. values of velocity fluctuations u' and v' and also of Reynolds stress $\overline{u'v'}$. (△) $\beta = 1°$. (○) $\beta = 0°$. Re is approximately 6×10^6. Tests 12 and 13. Convergent half period.

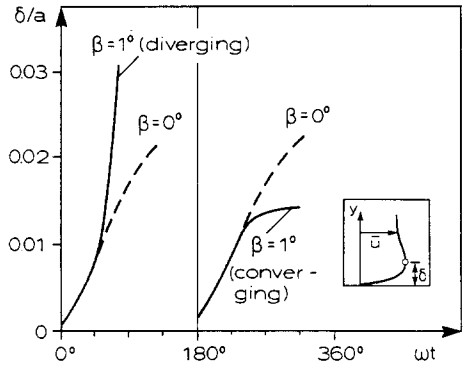

Fig. 17. Boundary layer thickness. $\beta=0°$ curve is taken from Sumer et al. (1987).

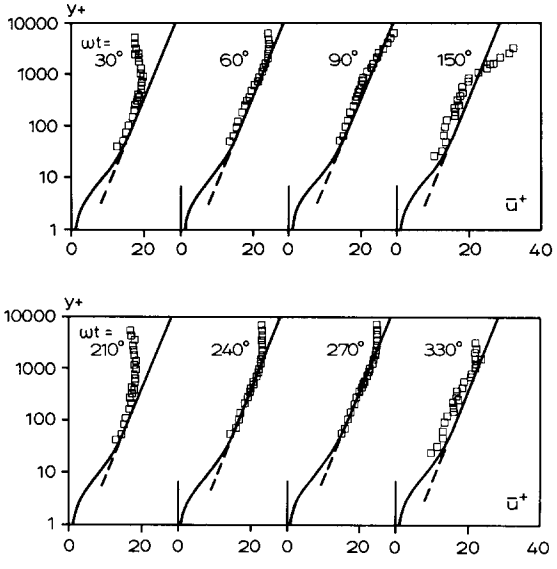

Fig. 18. Mean velocity distributions in semi-log plot for convergent–divergent boundary layer. $\beta=1°$. *Re* is approximately 6×10^6. Tests 10 and 12. (——) Eq. 14. (– – –) log law, $\bar{u}^+=2.5\ln y^+ + 5$.

factor ($=25$) (Van Driest, 1956). Note that $\bar{u}^+$ tends to the logarithmic distribution $\bar{u}^+=(1/\kappa)\ln y^+ + 5$ for large values of y^+, as seen from the figure (the dashed lines).

From the figure it can be observed that the u^+ versus y^+ variations in the present case are much the same as those reported in Jensen et al. (1989) for the case of non-diffusor flow ($\beta=0$).

Fig. 18 shows that the velocity distributions appear to satisfy the logarithmic law in both periods for quite some portion of the time. This may seem to

be somewhat unexpected, since it is known from the steady-flow research that the velocity distribution in a non-zero pressure-gradient flow, particularly in a diffusor type flow, may diverge in some degree from the familiar logarithmic law (see for example, McDonald, 1969). Various authors use different parameters to study the effect of pressure gradient on the velocity profile near the wall in steady flows. For example McDonald adopts the following parameter: $\alpha_0 = [\nu/(\rho U_f^3)](\mathrm{d}p/\mathrm{d}x)$.

The value of this parameter has been predicted to be in the order of magnitude of 0.001 for the phase value $\omega t = 90°$ in the present flow situation, and from McDonald's diagrams this value appears to be too small to have a significant effect on the logarithmic velocity distribution. A similar check was made against Engelund's (1981) theoretical solution, and this, too, indicated that the logarithmic velocity distribution is practically unaffected for the present flow situation.

4.4. Remarks regarding the application of the present results

When the wave boundary layer over a sloping bed under real waves is considered, there will be considerable changes with respect to what occurs in a convergent channel, the experimental flow environment in the present study. The real waves deform (namely, the wave heights increase) as they progress over the sloping bed (shoaling). Clearly, the present tunnel simulation does not reproduce this effect. Therefore, the present results can only be applicable in situations where no substantial shoaling occurs.

Secondly, the convergent/divergent geometry of the flow environment, both in the case of real waves over a sloping bed and in the case of oscillatory flow in a convergent tunnel, induces a streamwise pressure gradient. This pressure gradient, as seen from the present results, is central as regards the observed properties of the wave boundary layer, such as the streaming, the asymmetric behaviour of the wall shear stress in the two half periods, and the suppression and enhancement of the turbulence. Obviously, the pressure gradient induced in the convergent tunnel is not precisely the same as that induced over a sloping bed in real waves. Unfortunately, no pressure measurements have been made in the experimental tunnel. However, comparison made on the basis of potential flow velocity variation $U/U_{0m} = (r_0/r)\sin(\omega t)$ in the tunnel and the linear wave theory showed that the pressure gradient experienced over the sloping bed under real waves could be simulated fairly well in the convergent tunnel.

Thirdly, the present results were obtained for the case of smooth wall (this constraint was imposed by the use of a hot-film probe to measure the wall shear stress). So, where the sea bed behaves like a rough boundary, caution must be exercised with regard to the implementation of the present results. One may note, however, that the situation where the seabed behaves like a

hydraulically smooth wall are not extremely rare. The bed covered with marine clay may be regarded as a hydraulically smooth bed. Also, in the case where the bed roughness is such that a/k_s is extremely large (k_s being the Nikuradse's sand roughness), then again the bed, with the combination of large Reynolds number, may behave like a hydraulically smooth boundary (Jensen et al., 1989).

Fourthly, the Reynolds number is one other parameter which needs to be taken into account, with regard to the extrapolation of laboratory results to real waves. The Reynolds numbers of the present tests are maintained quite large, within the range of *Re* encountered in practice. Therefore, as far as *Re* is concerned, there should be no problem, when the implementation of the present results to real waves is considered.

Finally, one last factor in the tunnel simulation of real waves over a sloping bed concerns the parameter a/D, referred to in section 4.2. This parameter was in the present tests in the order of magnitude of $a/D=O(10)$, while, in real-life situations, it may be in the order of magnitude of $a/D=O(1)$. (Obviously, the present experiments are unable to reproduce the field values of a/D due to the experimental constraints). Therefore, here too, caution must be exercised when extrapolating the present results to real waves. The trends as regards this parameter are not conclusive in the present report, as the covered range of a/D is too narrow, as mentioned previously. However, for this, reference may be made to Justesen (1988a) where the friction coefficients and the period-averaged wall shear stress are given as function of a/k_s for a given value of D/k_s.

5. CONCLUSIONS

(i) In turbulent oscillatory boundary-layer flows in a convergent–divergent channel, there exists a constant, non-zero, period-averaged flow near the wall (the streaming) which occurs in the direction of convergence. This flow is balanced with a counter flow in the core region of the convergent–divergent channel. The magnitude of the streaming increases with the angle of divergence of the channel.

(ii) The friction coefficient in the convergent half period increases with the angle of divergence of the channel. The opposite is true for the divergent half period.

(iii) Turbulence is greatly suppressed in the convergent half period of the flow. The suppression of turbulence is so strong that its effect is felt even in the divergent half period for some portion of the time (up to about $\omega t=60°$ for the case studied in the present work). After the turbulence recovers in the divergent half period, an immense growth occurs in the turbulence quantities.

(iv) The boundary layer is rather thick in the divergent half period, while the opposite is true for the convergent half period of the flow.

(v) The familiar logarithmic layer is present in both the convergent and the divergent half periods in much the same way as it is in a non-diffusor ($\beta=0°$) boundary-layer flow. However, for larger values of the divergence angle (namely, $\beta>1°$), this may not be the case.

ACKNOWLEDGEMENTS

The study is partially supported by the research programme "Marine Technique" of the Danish Scientific Council (STVF) and by the Commission of the European Communities, Directorate General for Science, Research and Development under MAST Contracts No. 0035-C and MAS 2 CT 92-0027. We thank Dr. Bjørn L. Jensen and Mr. E.A. Rossen, M.Sc., who have been involved at various stages in the work presented in this paper.

REFERENCES

Davies, A.G., Soulsby, R.L. and King, H.L., 1988. A numerical model of the combined wave and current bottom boundary layer. J. Geophys. Res., 93.

Engelund, F., 1973. Analogy between the velocity distribution in a stable atmosphere and in divergent channels. Phys. Fluids, 16(10).

Engelund, F., 1981. Energy and momentum equation for non-uniform flow. Series Paper No. 29, Inst. of Hydrodynamics and Hydraulic Eng., Technical University of Denmark.

Hagatun, K. and Eidsvik, K.J., 1986. Oscillating turbulent boun dary layers with suspended sediment. J. Geophys. Res., 91(C11): 13045–13055.

Hino, M., Kashiwayanagi, M., Nakayama, A. and Hara, T., 1983. Experiments on the turbulence statistics and the structure of a reciprocating oscillatory flow. J. Fluid Mech., 131: 363–400.

Jensen, B.L., Sumer, B.M. and Fredsøe, J., 1989. Turbulent oscillatory boundary layers at high Reynolds numbers. J. Fluid Mech., 206: 265–297.

Jonsson, I.G., 1968. Plane-wall diffuser flow. Coastal Memo No. 1, Coastal Engineering Laboratory, (now Inst. of Hydrodyn. and Hydraul. Eng.), Technical University of Denmark.

Justesen, P., 1988a. Turbulent Wave Boundary Layers. Thesis submitted as one of the requirements for the Degree of Lic. Tech. (the Danish Ph.D.), Inst. Hydrodyn. and Hydraul. Eng., Technical University of Denmark.

Justesen, P., 1988b. Prediction of turbulent oscillatory flow over rough beds. Coastal Eng., 12: 257–284.

Kader, B.A. and Yaglom, A.M., 1978. Similarity treatment of moving equilibrium turbulent boundary layers in adverse pressure gradient. J. Fluid Mech., 89(2): 305–342.

Kamphuis, J.W., 1975. Friction factor under oscillatory waves. J. Waterw. Port Coastal Ocean Eng. Div. ASCE, 101(WW2): 135–144.

Longuet-Higgins, M.S., 1953. Mass transport in water waves. Philos. Trans. R. Soc. London, Ser. A, 245(903): 535–581.

Longuet-Higgins, M.S., 1957. The mecahnics of the boundary-layer near the bottom in a progressive wave. Appendix to Russell, R.C. H. and Osorio, J.D.C.: An experimental investigation of drift profiles in a closed channel. In: Proc. 6th Int. Conf. Coastal Eng., Miami, FL, pp. 184–193.

McDonald, H., 1969. The effect of pressure gradient on the law of the wall in turbulent flow. J. Fluid Mech., 35(2): 311–336.
Sleath, J.F.A., 1987. Turbulent oscillatory flow over rough beds. J. Fluid Mech., 182: 369–409.
Sumer, B.M., Jensen, B.L. and Fredsøe, J., 1987. Turbulence in oscillatory boundary layers. In: G. Comte-Bellot and J. Mathieu (Editors), Advances in Turbulence. Springer Verlag, Berlin, pp. 556–567.
Townsend, A.A., 1961. Equilibrium layers and wall turbulence. J. Fluid Mech., 11(1): 97–120.
Van Driest, E.R., 1956. On turbulent flow near a wall. J. Aeronaut. Sci., 23: 1007–1011.